

EVN observations of eleven GHz-Peaked-Spectrum radio sources at 2.3/8.4GHz

L. Xiang¹, D. Dallacasa^{2,4}, P. Cassaro³, D. Jiang⁵, and C. Reynolds⁶

¹ National Astronomical Observatories, Chinese Academy of Sciences, 40-5 South Beijing Road, Urumqi 830011, China
e-mail: liux@ms.xjb.ac.cn

² Dipartimento di Astronomia, Università di Bologna, via Ranzani 1, I-40127 Bologna, Italy
e-mail: dallacasa@ira.cnr.it

³ Istituto di Radioastronomia del CNR, C.P. 141, I-96017 Noto SR, Italy
e-mail: cassaro@noto.ira.cnr.it

⁴ Istituto di Radioastronomia del CNR, via P. Gobetti 101, 40129 Bologna, Italy

⁵ Shanghai Astronomical Observatory, Chinese Academy of Sciences, 80 Nandan Road, Shanghai 200030, China
e-mail: djiang@shao.ac.cn

⁶ Joint Institute for VLBI in Europe, Postbus 2, 7990 AA Dwingeloo, The Netherlands
e-mail: reynolds@jive.nl

Received 3 August 2004 / Accepted 17 December 2004

Abstract. We present results of EVN observations of eleven GHz-Peaked-Spectrum (GPS) radio sources at 2.3/8.4 GHz. These sources are from the classical "bright" GPS source samples with peak flux densities > 0.2 Jy and spectral indices $\alpha < -0.2$ ($S \propto \nu^{-\alpha}$) in the optically thick regime of their convex spectra. Most of the target sources did not have VLBI images at the time this project started. The aim of the work is to find Compact Symmetric Object (CSO) candidates from the "bright" GPS samples. These CSOs play a key role in understanding the very early stage of the evolution of individual radio galaxies. The reason for investigating GPS source samples is that CSO candidates are more frequently found among this class of radio sources. In fact both classes, GPS and CSO, represent a small fraction of the flux limited and flat-spectrum samples like PR+CJ1 (PR: Pearson-Readhead survey, CJ1: the first Caltech-Jodrell Bank survey) and CJF (the Caltech-Jodrell Bank flat spectrum source survey) with a single digit percentage progressively decreasing with decreasing flux density limit. Our results, with at least 3, but possibly more CSO sources detected among a sample of 11, underline the effectiveness of our approach. The three confirmed CSO sources (1133+432, 1824+271, and 2121-014) are characterized by a symmetric pair of resolved components, each with steep spectral indices. Five further sources (0144+209, 0554-026, 0904+039, 0914+114 and 2322-040) can be considered likely CSO candidates. The remaining three sources (0159+839, 0602+780 and 0802+212) are either of core-jet type or dominated by a single component at both frequencies.

Key words. galaxies: nuclei – quasars: general – radio continuum: galaxies

1. Introduction

Compact Symmetric Objects (CSOs) are a class of radio sources with distinctive radio properties. They are powerful and compact sources with overall size < 1 kpc, dominated by lobe/jet emission on both sides of the central engine, and are thought to be relatively free of beaming effects (Wilkinson et al. 1994). Their small size is most likely due to their youth ($< 10^4$ years) and not due to a dense confining medium (Owsianik & Conway 1998). A unification scenario assumes that CSOs evolve into Medium-size Symmetric Objects (MSOs, 1-15 kpc), which, in turn, evolve into Large Symmetric Objects (LSOs, > 15 kpc), i.e. large FR II radio sources (Fanti et al. 1995, Readhead et al. 1996, Taylor 2003).

CSOs are of particular interest in the study of the physics and evolution of active galaxies. First, CSO activity may be triggered through galaxy-galaxy merging, and the host galaxies of some CSOs exhibit merging or interaction diagnostics (Xiang et al. 2000, Perlman et al. 2001). A few CSOs have been found in known merging systems, e.g. 1345+125 (Xiang et al. 2002, Lister et al. 2003). Second, hot-spot proper motions from $0.1c$ to $0.8c$ have been detected in CSOs (Fanti 2000 and references therein, Polatidis & Conway 2003, Kellermann et al. 2004), and the estimated ages are between 100 and a few thousand years. A statistical study of the hot-spot proper motions and ages will be useful to pursue the CSO evolution from the very beginning of its radio burst. Third, CSOs inhabit the densest parts of their host galaxies (in other words, the nuclear regions of galaxies), and as such provide excellent probes of the

ambient medium of the active galactic nuclei through e.g. HI absorption, free-free absorption (FFA) and the Thomson scattering effect (Taylor 2003, Pihlström et al. 2003, Xiang 2004).

However, only a few CSOs have been well explored, which is not enough for a statistically sound study. The first systematic search for CSOs among the population of VLBI radio sources was carried out on the Pearson and Readhead (PR, Pearson & Readhead 1988) and the first Caltech–Jodrell Bank (CJ1, Xu et al. 1995) VLBI surveys. Together they form a flux limited complete sample of 200 sources with $S_{5\text{GHz}} > 0.7$ Jy and $\delta > 35^\circ$. A total of 14 CSOs were found (Polatidis et al. 1999) with a fractional incidence of 7%. If we consider also the second Caltech–Jodrell Bank VLBI survey (CJ2, Henstock et al. 1995) and the Caltech–Jodrell Bank Flat spectrum source survey (CJF, Taylor et al. 1996), the fraction goes down to 4.4% (18 CSOs out of 411 radio sources). If we finally consider also the VLBA Calibrator Survey we obtain 39 CSOs out of 1900 radio sources (2.1%).

The CSO detection rate appears to decrease as the sample size increases by lowering the flux density limit, i.e. there seems to be a trend to lower CSO incidence among fainter sources. On the other hand, the CJ2, CJF and VCS samples are defined as flat spectrum sources with spectral indices $\alpha < 0.5$ (we use $S \propto \nu^{-\alpha}$ in this paper). In contrast, a half of the CSOs in the flux limited complete sample, PR+CJ1, show steep spectra of $\alpha > 0.5$. Therefore, steep spectrum CSOs will be missed in the flat spectrum samples.

GPS (GHz-Peaked-Spectrum) radio sources are a significant fraction of the bright (centimeter-wavelength-selected) radio source sample ($\approx 10\%$) but they are not well understood. The GPS sources are powerful ($P_{1.4\text{GHz}} \geq 10^{25} \text{WHz}^{-1}$), compact (≤ 1 kpc) and have convex radio spectra that peak between about 0.5 and 10 GHz (observer’s frame). Only about 12% of GPS sources show extended radio emission (> 1 kpc), and it is diffuse and very faint. Most GPS sources appear to be truly compact and isolated (see O’Dea 1998 for a review of the GPS source properties).

It is found that, of 14 detected CSOs in the PR+CJ1 sample, 10 are GPS radio sources. Furthermore, six out of 10 GPS-type CSOs have shown steep spectra with spectral indices of $\alpha > 0.5$ in their optically thin regime, and their cores are relatively weak. Given that these CSOs are small radio sources, it is quite likely that their low frequency radio emission will be absorbed due to either Synchrotron Self Absorption (SSA), or Free-Free absorption, giving rise to a peaked (GPS) radio spectrum. This is why a number of CSOs in the PR+CJ1 sample are GPS sources. Hence, searching in GPS samples would be an efficient way to find CSO sources.

GPS radio sources are usually identified with galaxies at low to intermediate redshift ($z < 1$), while quasars are at higher redshift (Snellen et al. 1999). Some GPS radio sources have no optical counterparts yet, and these empty fields are likely to be distant galaxies, too faint to be detected. A strong correlation between the milliarcsecond morphology and the optical host in bright GPS sources suggests that galaxies are generally associated with CSOs while quasars have more often a core-jet or complex morphology (Stanghellini et al. 1998).

There are a few tens of sources in bright GPS source samples, and a few of them have never (or poorly) been imaged with VLBI. From the lists of the bright GPS source samples (O’Dea et al. 1991, 1996, de Vries et al. 1997), we have selected a number of sources to be imaged with VLBI. The first observation run was made at 1.6, 2.3 and 8.4 GHz with the EVN and MERLIN for 10 sources. From these multi-frequency high resolution images we found 2 CSOs and 4 CSO candidates (Xiang et al. 2002).

In the following we present results from the second run with the EVN at 2.3 GHz and at 8.4 GHz. We observed the sources with peak flux densities > 0.2 Jy, spectral indices $\alpha < -0.2$ in the optically thick regime of their convex spectra, and absent or insufficient morphological information in the literature, so that a proper classification was not available.

Our search for CSOs from GPS samples is a complementary to that of the COINS group (Peck & Taylor 2000) which looks for CSOs based on samples consisting mainly of flat spectrum radio sources.

2. Observations and data reduction

The observations were carried out on 4 June 2002 at 2.3/8.4 GHz using the MKIV recording system with a bandwidth of 16 MHz at each frequency, in right circular polarization. The EVN antennae participating in this experiment were those located at Effelsberg, Wettzel, Medicina, Noto, Matera, Onsala, Yebes, Urumqi and Shanghai. All stations produced useful fringes. Snapshot observations of the 11 target sources (see Table 1) for a total of 24 hours were carried out. OQ208 and BL Lac were observed as calibration sources. In January 2003, the data correlation was performed at the VLBI correlator at the Joint Institute for VLBI in Europe in Dwingeloo.

The Astronomical Image Processing System (AIPS) software was used for editing, a-priori calibration, fringe-fitting, self-calibration and imaging. The AIPS procedure UVCRS was used to derive the antenna gains of Wettzel and Matera for which appropriate system temperature measurements were not available.

The absolute flux density scale is estimated to be accurate to about 10% based on the calibrator source OQ208. The amplitude of OQ208 on the shortest baseline Effelsberg–Wettzel was found to be 1.75 Jy at 2.3 GHz, and 2.0 Jy at 8.4 GHz in our calibrated data. The source is not resolved on this baseline, and these values are consistent with 1.65 Jy at 2.3 GHz, and 1.95 Jy at 8.4 GHz (Stanghellini et al. 1998) within an error of 5%. This source is believed not to have varied substantially at 2.3 GHz and at 8.4 GHz in recent years (Stanghellini et al. 1997); the flux density at 8.55 GHz measured at Effelsberg in May 2001 is 2.03 ± 0.10 Jy (A. Kraus, priv. communication). For most sources we obtained the final images using near-natural weighting of the visibilities in order to have a better sensitivity to larger source components.

3. Results and comments on sources

In this section we present and briefly highlight the results from the dual frequency VLBI observations.

Some basic information on the target sources is presented in Table 1. The source component parameters as measured on the VLBI images are summarized in Table 2. In the following we consider a possible interpretation of each source based on the morphology and the spectral properties derived from the data presented here.

3.1. PKS 0144+209 (JVAS 0146+2110, NVSS J014658+211024)

This radio source does not have an optical counterpart and is reported as an empty field in Table 1. Snellen et al. (2002) estimated its APM (the Automated Plate Measurement Facility at Cambridge) red magnitude is > 20 , and the APM blue magnitude is > 22 based on the digitized Palomar Observatory Sky Survey (POSS) plates.

In the Jodrell Bank–VLA Astrometric Survey (JVAS), the total flux density at 8.4 GHz for the source is 337.2 mJy and the source is classified as suitable (i.e. pointlike at subarcsecond resolution) as a MERLIN phase calibrator (Wilkinson et al. 1998). It was not detected at 22 GHz with the single dish in Metsähovi (Teräsraanta et al. 2001).

The VLBI images exhibit an elongated structure with a position angle of $\sim -40^\circ$. At 2.3 GHz (Fig. 1), the total source size detected is more extended to the North-West than at 8.4 GHz (Fig. 2). The source is also found in the VLBA Calibrator Survey (VCS, Beasley et al. 2002). A 2.3 GHz image is available from the VCS web page, which is similar in structure to our image. The source is a core-jet source if its southern end is the core of the source. However, if the strongest central component is the core, the source could be a CSO instead. The total flux density accounted for in our image at 8.4 GHz is $\sim 90\%$ of the JVAS measurement.

3.2. 0159+839 (JVAS J0207+8411, NVSS J020713+841111)

Spoelstra et al. (1985) classified this object as a 17th magnitude ‘stellar’ object, de Vries et al. (2000) marked the object as a ‘quasar?’. This is a ROSAT source, 1RXS J020716.5+841126.

In the radio, the JVAS flux density at 8.4 GHz is 77.9 mJy and the source is a suitable MERLIN phase calibrator (Wilkinson et al. 1998). Our VLBI images show a weak, slightly resolved source at 2.3 GHz (Fig. 3), and a point-like object at 8.4 GHz (Fig. 4, where about a half of the JVAS flux density is accounted for). The source is resolved into core-jet like (components A,B), and a hint of a third component C in the direction of the jet, while it is unresolved at 8.4 GHz. Further, the VLBI structure as a whole has an inverted spectral index ($\alpha = -0.38$). The spectrum becomes even more inverted ($\alpha = -0.86$) if we consider that the component seen at 8.4 GHz corresponds to the more compact component (A) at 2.3 GHz. A possible explanation for the different morphologies at 2.3 GHz and at 8.4 GHz is that the components A and B represent a core-jet source, with only the inverted spectrum core component being detected at 8.4 GHz. The jet component, with a

more optically thin synchrotron spectrum, is undetected at 8.4 GHz due to the low dynamic range of the image.

3.3. PKS 0554–026 (NVSS J055652–024105)

This is a galaxy with $m_V=18.5$ and redshift 0.235 (de Vries et al. 2000). Both VLBI images (Fig. 5 and Fig. 6) presented here show a structure where a series of well resolved components are aligned in the East-West direction. There is no indication of a possible core candidate. Based on these data a proper classification of this source is not possible, although it may be still considered a CSO candidate.

3.4. 0602+780 (JVAS J0610+7801, NVSS J061024+78013)

This object is identified as a very faint galaxy by Stanghellini et al. (1993). In the radio, the JVAS flux density at 8.4 GHz is 124.1 mJy and the source is a suitable MERLIN phase calibrator (Wilkinson et al. 1998). In the VCS it is found to be point source. Our images at both frequencies show a point-like source (Fig. 7 and Fig. 8), with a rather inverted spectrum ($\alpha = -0.57$). About 15% of the JVAS flux density is not accounted for in the VLBI image of Fig. 8, possibly related to a jet component completely resolved out by the present observations at both frequencies.

3.5. PKS 0802+212 (JVAS J0805+2106, NVSS J080538+210651)

The source is identified as a galaxy with $m_R=22.5$ (de Vries et al. 2000). In the radio, the JVAS flux density at 8.4 GHz is 348.8 mJy and the source is a suitable MERLIN phase calibrator (Wilkinson et al. 1998). The source was detected with a total flux density of 0.22 Jy at 22 GHz by Teräsraanta et al. (2001). Images at 2.3 GHz and at 8.4 GHz are available from the VCS. Our VLBI image at 2.3 GHz (Fig. 9) shows a marginally resolved object, whose structure is well highlighted at 8.4 GHz (Fig. 10) where a compact core-jet morphology is visible. Both our images are consistent with the VCS results. Indeed the total flux density accounted for in the 8.4 GHz image exceeds the VLA measurement of the JVAS by about 17%. There are also other signatures of a similar flux density variability if we compare the total flux density detected at 1.4 GHz in the NVSS and the FIRST (about 18% weaker). All these pieces of information suggest a core-jet classification for this source.

3.6. PKS 0904+039 (NVSS J090641+034242)

The source is identified with a galaxy, $m_I=22.1$, which appears slightly extended in an I band image. This object seems to be located in a small group of objects (presumably galaxies, de Vries et al. 2000).

In the radio, some extended emission to the South is visible in the NVSS image. However, the FIRST image of the same area shows that it is likely due to an unrelated background/foreground object. Indeed PKS 0904+039 is slightly

Table 1. GPS sources. Columns 1 through 14 provide source name, optical identification (G: galaxy, Q: quasar, EF: empty field; a '?' means that the classification is uncertain), optical magnitude and filter, redshift (* is a photometric estimate by Heckman et al. 1994), linear scale factor pc/mas [$H_0=100\text{km/s}$ and $q_0 = 0.5$ have been assumed], maximum VLBI angular size in mas, maximum VLBI linear size in pc, 2.7 GHz flux density in Jy from the NASA/IPAC Extragalactic Database (NED), source spectral index from our VLBI images, low frequency (optically thick) spectral index, high frequency (optically thin) spectral index, turnover frequency in GHz, peak flux density in Jy and references for the spectral information (ref: 1, de Vries et al. 1997; 2, Stanghellini et al. 1998).

source	id	m	z	pc/mas	θ mas	L pc	$S_{2.7}$ Jy	α_{vlbi}	α_l	α_h	ν_m GHz	S_m Jy	ref
0144+209	EF				50		0.85	0.87	-0.63	0.59	1.3	1.2	1
0159+839	Q?	17V			90			-0.38	-0.47	0.91	5.0	0.2	1
0554-026	G	18.5V	0.235	2.37	30	71	0.62	1.25	-1.07	0.63	1.0	0.8	1
0602+780	G	22.0R	1.1*	4.3	<25	<108		-0.57	-0.58	0.57	5.0	0.2	1
0802+212	G	22.5R			25		1.03	0.50	-0.54	0.57	1.8	1.0	1
0904+039	G	22.1I			80		0.44	1.72	-0.23	0.83	0.8	1.0	1
0914+114	G	20.0r	0.178	1.95	150	293	0.31	2.0	-0.1	1.6	0.3	2.3	2
1133+432	EF				40			1.37	-0.60	0.6	1.0	1.4	1
1824+271	G?	22.9R			45		0.23	1.43	-0.39	0.75	1.0	0.4	1
2121-014	G	23.3R	1.158	4.3	88	378	0.64	1.11	-0.56	0.75	0.5	1.8	1
2322-040	G	23.5R			65		0.91	1.36	-0.42	0.75	1.4	1.3	1

resolved in the FIRST survey and with a total flux density exceeding by about 10% the one measured in the NVSS.

The VLBI image at 2.3 GHz (Fig. 11) shows a series of resolved components roughly aligned p.a. -140° with a possible additional weak component to the South. Our image at 8.4 GHz (Fig. 12) detects three blobs in which component A in Fig. 11 is resolved. None of them is particularly compact enough to be considered as the source core. More than 50% of the total flux density at this frequency (cf. Stanghellini et al. 1998) is not accounted for in the VLBI image. Conversely, at 2.3 GHz the total flux density accounted for in our VLBI image slightly exceeds the literature data. We can consider this source a CSO candidate.

3.7. PKS 0914+114 (NVSS J091716+111336)

This source is associated with a galaxy, $m_r=20.0$ (Stanghellini et al. 1993), $z=0.178$ (de Vries et al. 1998). Our VLBI image at 2.3 GHz (Fig. 13), accounting for the whole source flux density at this frequency, shows four well separated components, with no obvious interpretation of the structure. Only one of them, likely component C, is detected at 8.4 GHz (Fig. 14). About 50% of the total flux density at this frequency (cf. Stanghellini et al. 1998) is missing in the image. If it is the component C, its spectral index would be $\alpha = 1.73$, slightly steeper than the optically thin spectral index ($\alpha = 1.6$) derived from VLA data. Given this steep spectral index and the source structure seen in our data, we can consider this object a CSO candidate.

3.8. B3 1133+432 (NVSS J113555+425844)

This is an empty field in the optical (Stickel et al. 1994). Our VLBI images at 2.3 GHz and at 8.4 GHz (Fig. 15 and Fig. 16) show a double source, with both components resolved by the

present observations. This source has been studied in detail by Dallacasa et al. (2002) at 1.7 GHz and by Orienti et al. (2004) at 5.0 GHz and at 8.4 GHz with the VLBA, as part of a study on the Compact Steep Spectrum sources from the B3-VLA sample selected by Fanti et al. (2001). Our results are consistent with the aforementioned papers, although our 8.4 GHz image could not account for about 35% of the total flux density. The spectral indices we derived for our components between 2.3 and 8.4 GHz ($\alpha = 1.23$ and $\alpha = 1.65$) are steeper than those derived by Orienti et al. (2004) between 5.0 and 8.4 GHz due to the smaller fraction of flux density accounted for in our 8.4 GHz image.

Despite the lack of a core detection, which would be one requirement for a proper CSO classification, we consider this object as a good CSO source, since we interpret the overall morphology as a very compact, lobe dominated double; to detect the core we would need a much higher dynamic range and possibly a better UV-coverage at 8.4 GHz.

3.9. 1824+271 (J1826+2707)

It is associated with a faint object with $m_R=22.9$ (O'Dea et al. 1990). Given such weak magnitude its optical counterpart does not have a morphological classification (G/Q) although galaxies are more frequently found than quasars associated with GPS sources. In the radio, our 2.3 and 8.4 GHz VLBI images (Fig. 17 and Fig. 18) show a double structure roughly aligned in the East-West direction; both components have steep spectra ($\alpha = 1.37$ for the brighter A component, $\alpha = 1.63$ for the weaker B component) and are consistent with the overall steep radio spectrum ($\alpha = 1.4$) derived from the literature data. In fact a flux density of 50 mJy at 8.085 GHz and of 230 mJy at 2.695 GHz are found in the NED database. These flux densities indicate that while the whole source flux density is accounted

Table 2. Parameters of the source components in the VLBI images at 2.3 and 8.4 GHz. The various columns provide: (1) source name and possible classification (CSOc: Compact Symmetric Object candidate, cj: core-jet), (2) total image intensity measured with IMEAN at 2.3 GHz, (3) component identification, (4) spectral index of component computed with *Sint*, (5),(6) peak (*Sp*) and integral intensity (*Sint*) of component at 2.3 GHz measured with JMFIT, (7),(8) major/minor axes and position angle of component at 2.3 GHz measured with JMFIT, (9) total image intensity measured with IMEAN at 8.4 GHz, (10) component identification, (11),(12) peak and integral intensity of component at 8.4 GHz measured with JMFIT, (13),(14) major/minor axes and position angle of component at 8.4 GHz measured with JMFIT.

Name class	$S_{2.3}$ mJy	α_c	Sp mJy	$Sint$ mJy	$\theta_1 \times \theta_2$ mas	PA °	$S_{8.4}$ mJy	Sp mJy	$Sint$ mJy	$\theta_1 \times \theta_2$ mas	PA °	
0144+209 CSOc	903						293	A B C	47 113 39	67.8 168 80	2.2×0.7 2.3×0.8 4.0×0.8	132 155 137
0159+839 cj	23	A B C	-0.86	12 9.0 4.3	12.2 21.6 5.8	4.6×4.6 19×3.4 7.4×3.4	0	A	31	37	1.1×0.9	106
0554-026 CSOc	275	A B	0.69	80.2 76.2	116.6 129.5	5.6×2.2 7.1×2.6	6.3	A1 A2 B	15 7.7 11	35 13 28	2.3×0.9 3.5×0.5 1.5×1.1	29 6 63
0602+780 cj	50			44.1	48.6	4.8×3.0	112		93	104	0.8×0.6	127
0802+212 cj	755						409	A B	263 71	293 140	0.5×0.3 1×1	7.8 144
0904+039 CSOc	508	A B C		271 82 23	367 112 56	11×2.7 11×5.2 32×9.7	37	A1 A2 A3	17 7.4 3.1	24 15 8.6	1.6×1.1 2.6×1.3 3.5×2.0	138 95 99
0914+114 CSOc	321	A B C D		43 22 190 18.5	46 31 214 27	5×5 6.5×5.3 4×1.8 7.7×3.7	0					
1133+432 CSO	1068	A B	1.23	557 282	692 367	3.4×1.5 3.8×2.2	92	A B	116 28	141 44	1.2×0.9 1.9×1.7	74 128
1824+271 CSO	222	A B	1.37	118 31	163 58	6.4×1.2 12×12	97	A B	24 5.4	28 7.1	1.7×1.1 2.0×1.4	116 129
2121-014 CSO	604	A B C	1.43	236 43 151	253 164 237	2.9×0.6 27×1.3 7.8×4.1	113	A C	145 26 67	145 40 103	3.5×2.6 3.5×2.6 3.6×1.6	81 81 46
2322-040 CSOc	956	A B	1.1	536 129	662 234	3.2×1.6 6.7×2.2	109	A ?	166 ?	160 ?	1.4×0.5 1.4×0.5	102 102

for in our 2.3 GHz VLBI image, some fraction of the flux density may be missing in our 8.4 GHz VLBI image.

The source structure is consistent with the expectation of a CSO seen in low dynamic range images, and therefore we suggest this classification.

3.10. PKS 2121-014 (NVSS J212339-011234)

This is a galaxy with $m_R=23.3$, which shows double structure presumably indicating a case of close interaction (de Vries et al. 2000). The redshift for this system is 1.158 (Snellen et al. 1996).

Our VLBI images exhibit a double structure with both components well resolved. At 2.3 GHz (Fig. 19) a second component may be added to the main one (component A), possibly representing a sort of tail/lobe emission. However, the component A is quite weak at 8.4 GHz (Fig. 20) with a spectral index of 1.43, indicating it is not the core of the source. Surprisingly,

component C has a mid-steep spectrum ($\alpha = 0.65$), despite its considerably larger size at 2.3 GHz. It is also possible that in the early data reduction the symmetrization caused by the fringe fitting process has been wrongly resolved, resulting in a swap of the position of the two components.

As in the case of 1824+271, we consider this source as a CSO.

3.11. PKS 2322-040 (NVSS J232510-034446)

This is a galaxy with $m_R=23.5$, which appears to be a regular elliptical and possibly a member of a small group of galaxies (de Vries et al. 2000).

Our VLBI images show a double structure at 2.3 GHz (Fig. 21), while only a single component is detected at 8.4 GHz. This component is slightly resolved (Fig. 22). The whole flux density is accounted for in the 2.3 GHz image, while at 8.4 GHz we can account for 166 mJy only, while a flux density of

240 mJy is reported at this frequency in the NED database. The missing flux density may be in the secondary component 'B' which is lost in our 8.4 GHz image due to poor UV coverage in the North-South direction (there is a negative beam sidelobe at the position of component 'B' in Fig.22 preventing us from collecting enough flux density in that area).

The spectral index for the component A is 1.1 (consistent with the spectral index of the whole source $\alpha = 1.16$, as measured from the NED values), indicating it is more likely a lobe rather than the core of the source.

The source 2322–040 can be considered a CSO candidate.

4. Discussion

CSOs are defined as very compact radio sources (a few hundreds of pc in size) whose radio emission is dominated by a pair of hot-spots and lobes lying on the opposite side of a core. The overall source spectrum has a convex shape as commonly found in GPS radio sources, and most if not all CSOs are found among GPSs or at least among peaked spectrum radio sources.

Ideally, a core component, with a flatter (often also inverted) spectrum than the hot-spots and lobes must be identified before a compact radio source can be confirmed as a CSO. For some CSOs with a jet axis very close to the plane of sky the core may be Doppler dimmed and become so weak as to be undetectable. However the CSO classification may be still valid if there are symmetric edge-brightened hot spots and/or extended lobes (Taylor & Peck 2003). Examples can be found in J1734+0926 (Peck & Taylor 2000) and in 1133+432, 1824+271 and 2121–014 presented in this paper.

The core of CSOs in some cases can become brighter at high frequencies, e.g. CSO 1946+708 (Taylor & Vermeulen 1997) due to a turnover frequency substantially higher than the lobes and the hot-spots. It is then possible to detect the core in CSOs at frequencies higher than 8.4 GHz. On the other hand, a few CSOs possess a relatively bright core at centimeter wavelengths (Peck & Taylor 2000), and they could be affected by Doppler boosting to some extent.

The flux densities at 2.3 GHz from our VLBI images account for the whole radio source emission as extrapolated by the 2.7 GHz literature data. All individual deviations can be referred to the amplitude calibration error. Most of the sources have steep radio spectra above 2.3 GHz, and the component spectral indices we found may be steeper than those reported by de Vries et al. (1997) since some amount of flux density is not accounted for in our VLBI images at 8.4 GHz, possibly due to the lack of short UV spacings.

Concerning the sources we classify as CSO or candidate, none of them has the core detected, possibly due to a limited image dynamic range and/or to an intrinsically weak core. The spectral index of the components detected in our image is generally very steep, often with $\alpha > 1$. This evidence coupled with the fact that all the components are well resolved in our VLBI images led us to consider them as possible CSO radio sources.

5. Summary and conclusions

Below we summarize the results and possible classification of the sources.

1) All sources we observed have been detected at 2.3/8.4 GHz. For some sources these are the first VLBI images allowing the study of the morphology with parsec scale resolution.

2) The sources 1133+432, 1824+271 and 2121–014 have radio emission coming from two well-resolved, steep spectrum regions with comparable flux density and therefore can be classified as bona-fide CSOs.

3) Other sources have a more complex structure: 0914+114 consists of 4 components at 2.3 GHz but only one is detected at 8.4 GHz, similarly 2322–040 is double at 2.3 GHz, but has a single component detected at 8.4 GHz. The sources 0144+209, 0554–026 and 0904+039 are resolved into a series of small components at both frequencies, all with rather steep spectra. Given the source complexity our observations could not provide a UV-coverage good enough to allow imaging of more details. We still consider these five sources as CSO candidates.

4) Of the remaining three sources, two (0159+839 and 0602+780) have a single, inverted spectrum component detected, while the third (0802+212) is marginally resolved at 2.3 GHz and shows a typical core-jet structure in our 8.4 GHz image.

A sound statistical study will be possible once the sources from the "bright" GPS samples have been well explored with VLBI.

Multi-frequency VLBI images are suited to do the spectral analysis of components in more detail. Further work is required on the CSO and CSO candidates presented here, and images at 5 GHz with a better sensitivity are necessary to confirm their classification.

Our images of 1133+432, 1824+271 and 2121–014 can be used in future studies aiming to measure hot-spot proper motion.

Acknowledgements. This work was supported by the Natural Science Foundation of China (NSFC) under grant No.19973014, No.10373019 and the fund with No. G1999075403. We thank the anonymous referee for important comments, and R. Ström and Z.-Q Shen for helpful comments. L.X. thanks Carlo Stanghellini for help with the proposal of this project, and L. Gurvits, M. A. Garrett and B. Campbell for help when L.X. was doing data calibration in JIVE. This research has made use of the NASA/IPAC Extragalactic Database (NED) which is operated by the Jet Propulsion Laboratory, Caltech, under contract with NASA.

References

- Beasley A. J., Gordon D., Peck A. B., Fomalont E. B., Ma C., 2002, ApJS 141, 13
- Dallacasa D., Tinti S., Fanti C., Fanti R., Gregorini L., Stanghellini C., Vigotti M., 2002, A&A 389, 115
- de Vries W. H., Barthel P. D., O'Dea C. P., 1997, A&A 321, 105
- de Vries W. H., O'Dea C. P., Perlman E., Lehnert M. D., Barthel P. D., 1998, ApJ 503, 138
- de Vries W. H., O'Dea C. P., Barthel P. D., Thompson D. J., 2000, A&AS 143, 181
- Fanti C., Fanti R., Dallacasa D., Schilizzi R. T., Spencer R. E., Stanghellini C., 1995, A&A 302, 317

- Fanti C., 2000, in Proceedings of 5th European VLBI Network Symposium, held at Chalmers Technical University, eds. A. G. Polatidis, R. S. Booth, & Y. Pihlström (Published by Onsala Space Observatory), p73
- Fanti C., Pozzi F., Dallacasa D., Fanti R., Gregorini L., Stanghellini C., Vigotti M. 2001, A&A 369, 380
- Heckman T. M., O’Dea C. P., Baum S. A., Laurikainen E., 1994, ApJ 428, 65
- Henstock D. R., Browne I. W. A., Wilkinson P. N., Taylor G. B., Vermeulen R. C., Pearson T. J., Readhead A. C. S., 1995, ApJS 100, 1
- Lister M. L., Kellermann K. I., Vermeulen R. C., Cohen M. H., Zensus J. A., Ros E., 2003, ApJ 584, 135L
- Kellermann K. I., Lister M. L., Homan D. C., Vermeulen R. C., Cohen M. H., Ros E., Kadler M., Zensus J. A., Kovalev Y. Y., 2004, ApJ 609, 539
- O’Dea C. P., Baum S. A., Stanghellini C., Morris G. B., Patnaik A. R., Gopal-Krishna, 1990, A&AS 84, 549
- O’Dea C. P., Baum S. A., Stanghellini C., 1991, ApJ 380, 66
- O’Dea C. P., Stanghellini C., Baum S. A., Charlot S., 1996, ApJ 470, 806
- O’Dea C. P., 1998, PASP 110, 493
- Orienti M., Dallacasa D., Fanti C., Fanti R., Tinti S., Stanghellini C. 2004, A&A 426, 463
- Owsianik I., Conway J. E., 1998, A&A 337, 69
- Pearson T. J., Readhead A. C. S., 1988, ApJ 328, 114
- Peck A. B., Taylor G. B., 2000, ApJ 534, 90
- Perlman E. S., Stocke J. T., Conway. J., Reynolds C., 2001, AJ 122, 536
- Pihlström Y. M., Conway J. E., Vermeulen R. C., 2003, A&A 404, 871
- Polatidis A., Wilkinson P. N., Xu W., Readhead A. C. S., Pearson T. J., Taylor G. B., Vermeulen R. C., 1999, NewAR 43, 657
- Polatidis A. G., Conway J. E., 2003, PASA 20, 69
- Readhead A. C. S., Taylor G. B., Pearson T. J., Wilkinson P. N., 1996, ApJ 460, 634
- Snellen I. A. G., Bremer M. N., Schilizzi R. T., Miley G. K., van Ojik R., 1996, MNRAS 279, 1294
- Snellen I. A. G., Schilizzi R. T., Bremer M. N., Miley G. K., de Bruyn A. G., Röttgering H. J. A., 1999, MNRAS 307, 149
- Snellen I. A. G., McMahon R. G., Hook I. M., Browne I. W. A., 2002, MNRAS 329, 700
- Stanghellini C., O’Dea C. P., Baum S. A., Laurikainen E., 1993, ApJS 88, 1
- Stanghellini C., Bondi M., Dallacasa D., O’Dea C. P., Baum S. A., Fanti R., Fanti C., 1997, A&A 318, 376
- Stanghellini C., O’Dea C. P., Dallacasa D., Baum S. A., Fanti R., Fanti C., 1998, A&AS 131, 303
- Stickel M., Kühr H., 1994, A&AS 103, 349
- Spiegelstra T. A. T., Patnaik A. R., Gopal-Krishna, 1985, A&A 152, 38
- Taylor G. B., 2003, NewAR 47, 585
- Taylor G. B., Peck A. B., 2003, ApJ 597, 157
- Taylor G. B., Vermeulen R. C., 1997, ApJ 485, L9
- Taylor G. B., Vermeulen R. C., Readhead A. C. S., Pearson T. J., Henstock D. R., Wilkinson P. N., 1996, ApJ 107, 37
- Teräsranta H., Urpo S., Wires S., Valtonen M., 2001, A&A 368, 431
- Wilkinson P. N., Polatidis A. G., Readhead A. C. S., Xu W., Pearson T. J., 1994, ApJ 432, L87
- Wilkinson P. N., Browne I. W. A., Patnaik A. R., Wrobel J. M., Sorathia B., 1998, MNRAS 300, 790
- Xiang L., 2000, in Proceedings of 5th European VLBI Network Symposium, held at Chalmers Technical University, eds. A. G. Polatidis, R. S. Booth, & Y. Pihlström (Published by Onsala Space Observatory), p87
- Xiang L., Stanghellini C., Dallacasa D., Haiyan Z., 2002, A&A 385, 768
- Xiang L., 2004, ChJAA, in press
- Xu W., Readhead A. C. S., Pearson T. J., Polatidis A. G., Wilkinson P. N., 1995, ApJS 99, 297

List of Objects

- ‘PKS 0144+209’ on page 3
- ‘JVAS 0146+2110’ on page 3
- ‘NVSS J014658+211024’ on page 3
- ‘0159+839’ on page 3
- ‘JVAS J0207+8411’ on page 3
- ‘NVSS J020713+841111’ on page 3
- ‘1RXS J020716.5+841126’ on page 3
- ‘PKS 0554–026’ on page 3
- ‘NVSS J055652–024105’ on page 3
- ‘0602+780’ on page 3
- ‘JVAS J0610+7801’ on page 3
- ‘NVSS J061024+78013’ on page 3
- ‘PKS 0802+212’ on page 3
- ‘JVAS J0805+2106’ on page 3
- ‘NVSS J080538+210651’ on page 3
- ‘PKS 0904+039’ on page 3
- ‘NVSS J090641+034242’ on page 3
- ‘0144+209’ on page 4
- ‘0159+839’ on page 4
- ‘0554–026’ on page 4
- ‘0602+780’ on page 4
- ‘0802+212’ on page 4
- ‘0904+039’ on page 4
- ‘0914+114’ on page 4
- ‘1133+432’ on page 4
- ‘1824+271’ on page 4
- ‘2121–014’ on page 4
- ‘2322–040’ on page 4
- ‘PKS 0914+114’ on page 4
- ‘NVSS J091716+111336’ on page 4
- ‘B3 1133+432’ on page 4
- ‘NVSS J113555+425844’ on page 4
- ‘1824+271’ on page 4
- ‘J1826+2707’ on page 4
- ‘0144+209’ on page 5
- ‘0159+839’ on page 5
- ‘0554–026’ on page 5
- ‘0602+780’ on page 5
- ‘0802+212’ on page 5
- ‘0904+039’ on page 5
- ‘0914+114’ on page 5
- ‘1133+432’ on page 5
- ‘1824+271’ on page 5
- ‘2121–014’ on page 5
- ‘2322–040’ on page 5
- ‘PKS 2121–014’ on page 5
- ‘NVSS J212339–011234’ on page 5
- ‘PKS 2322–040’ on page 5
- ‘NVSS J232510–034446’ on page 5

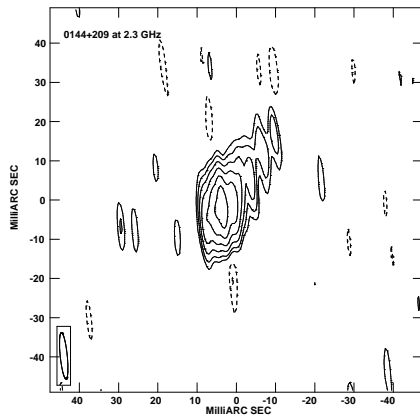


Fig. 1. 0144+209 at 2.3 GHz, the restoring beam is 11.8×1.8 mas in PA 5.8° , the rms noise on the image is 2 mJy/beam, the lowest contour is 2.5σ , the peak flux density is 286 mJy/beam. The contour levels here and the following figures are -1, 1, 2, 4, 8, 16, 32, 64, 128, 256, 512.

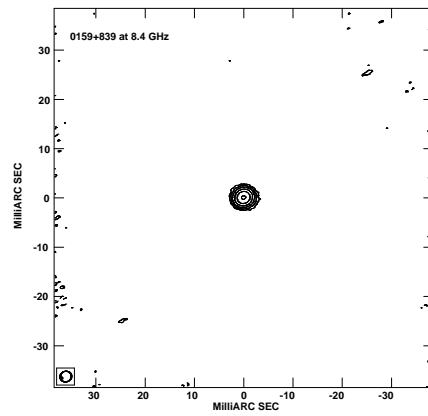


Fig. 4. 0159+839 at 8.4 GHz, the restoring beam is 2.3×2.1 mas in PA -67.6° , the rms noise on the image is 0.3 mJy/beam, the lowest contour is 2.0σ , the peak flux density is 31 mJy/beam.

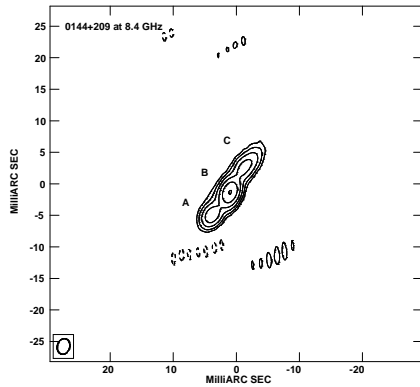


Fig. 2. 0144+209 at 8.4 GHz, the restoring beam is 2.5×2.0 mas in PA -15.4° , the rms noise on the image is 1.0 mJy/beam, the lowest contour is 3.5σ , the peak flux density is 114 mJy/beam.

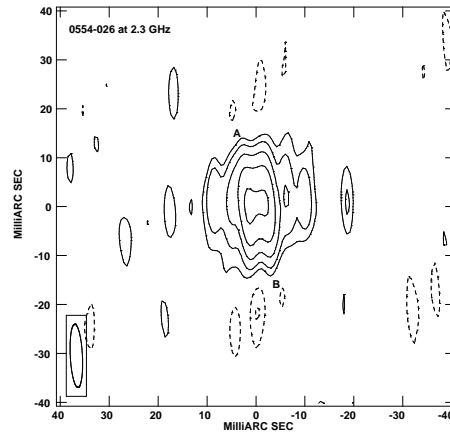


Fig. 5. 0554-026 at 2.3 GHz, the restoring beam is 12.8×2.5 mas in PA 2.9° , the rms noise on the image is 2.2 mJy/beam, the lowest contour is 2σ , the peak flux density is 86 mJy/beam.

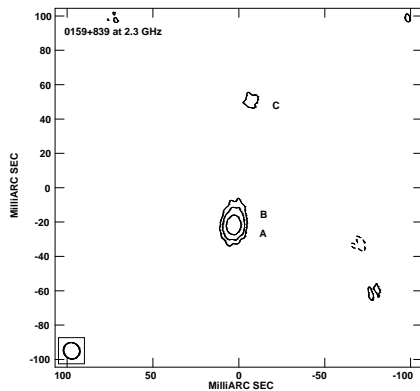


Fig. 3. 0159+839 at 2.3 GHz, the restoring beam is 9.8×9.2 mas in PA 39.3° , the rms noise on the image is 0.8 mJy/beam, the lowest contour is 3.7σ , the peak flux density is 20.5 mJy/beam.

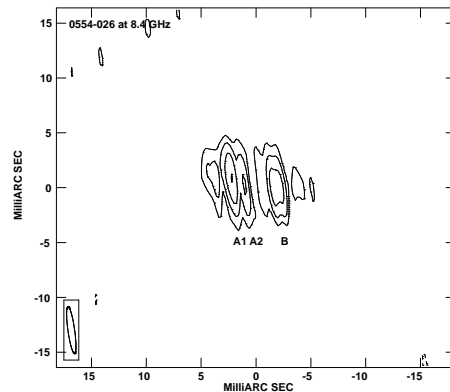


Fig. 6. 0554-026 at 8.4 GHz, the restoring beam is 4.3×0.6 mas in PA 8° , the rms noise on the image is 0.6 mJy/beam, the lowest contour is 3σ , the peak flux density is 15 mJy/beam.

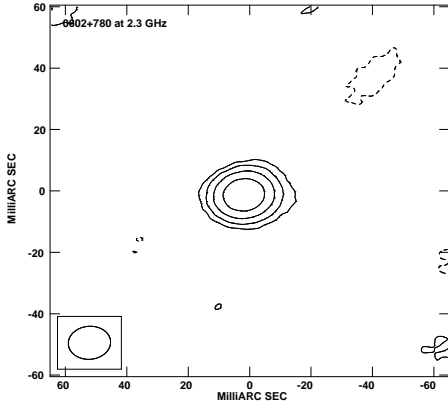


Fig. 7. 0602+780 at 2.3 GHz, the restoring beam is 13.8×10.7 mas in PA -85.5° , the rms noise on the image is 1.2 mJy/beam, the lowest contour is 2.5σ , the peak flux density is 44 mJy/beam.

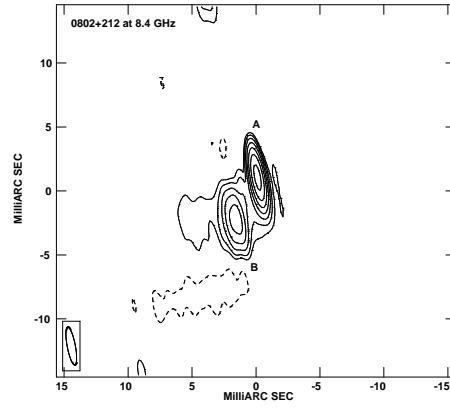


Fig. 10. 0802+212 at 8.4 GHz, the restoring beam is 3.1×0.7 mas in PA 10.7° , the rms noise on the image is 1.5 mJy/beam, the lowest contour is 2σ , the peak flux density is 264 mJy/beam.

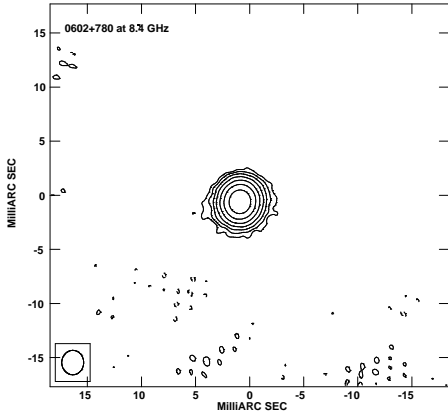


Fig. 8. 0602+780 at 8.4 GHz, the restoring beam is 2.3×2.0 mas in PA -0.6° , the rms noise on the image is 0.6 mJy/beam, the lowest contour is 1.3σ , the peak flux density is 94 mJy/beam.

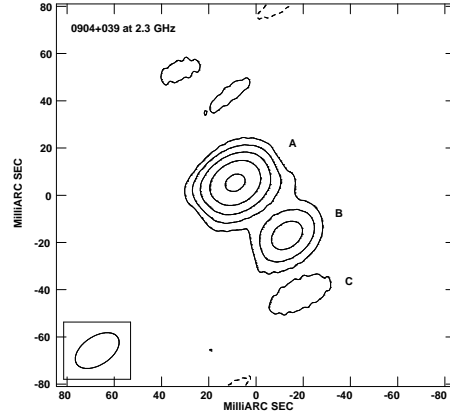


Fig. 11. 0904+039 at 2.3 GHz, the restoring beam is 20.7×12 mas in PA -57° , the rms noise on the image is 5.9 mJy/beam, the lowest contour is 2.5σ , the peak flux density is 273 mJy/beam.

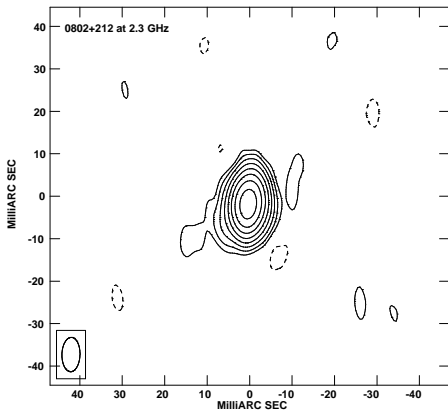


Fig. 9. 0802+212 at 2.3 GHz, the restoring beam is 8.1×4.3 mas in PA -1.5° , the rms noise on the image is 0.8 mJy/beam, the lowest contour is 3.7σ , the peak flux density is 618 mJy/beam.

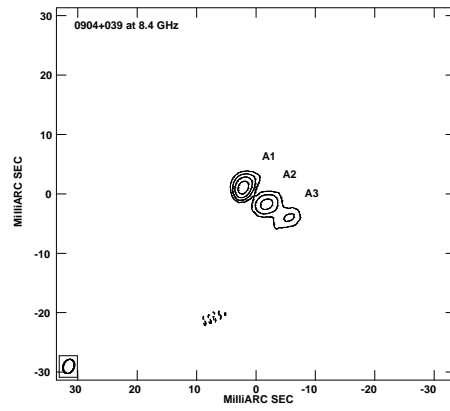


Fig. 12. 0904+039 at 8.4 GHz, the restoring beam is 2.5×1.8 mas in PA -21.3° , the rms noise on the image is 0.4 mJy/beam, the lowest contour is 3.5σ , the peak flux density is 17 mJy/beam.

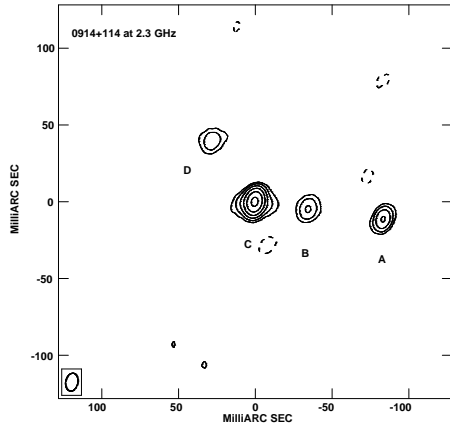


Fig. 13. 0914+114 at 2.3 GHz, the restoring beam is 12×7.8 mas in PA -11.2° , the rms noise on the image is 1.4 mJy/beam, the lowest contour is 3.6σ , the peak flux density is 126 mJy/beam.

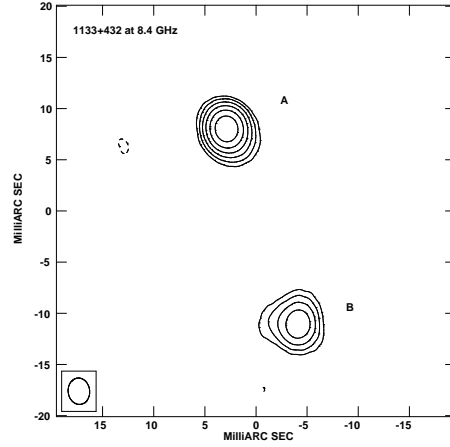


Fig. 16. 1133+432 at 8.4 GHz, the restoring beam is 2.6×2.1 mas in PA 6.6° , the rms noise on the image is 0.6 mJy/beam, the lowest contour is 3.3σ , the peak flux density is 117 mJy/beam.

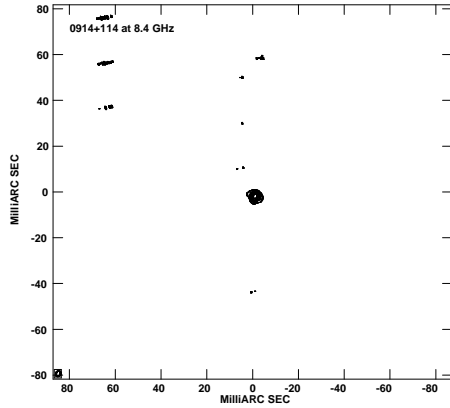


Fig. 14. 0914+114 at 8.4 GHz, the restoring beam is 2.5×1.9 mas in PA -18° , the rms noise on the image is 0.3 mJy/beam, the lowest contour is 2.7σ , the peak flux density is 20 mJy/beam.

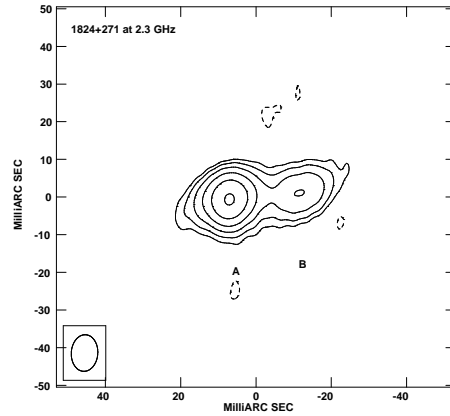


Fig. 17. 1824+271 at 2.3 GHz, the restoring beam is 9.5×6.7 mas in PA -3.6° , the rms noise on the image is 1.1 mJy/beam, the lowest contour is 3.6σ , the peak flux density is 137 mJy/beam.

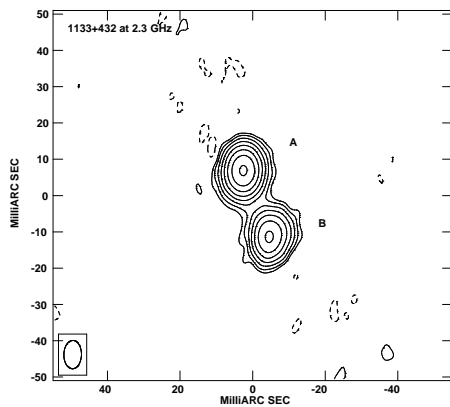


Fig. 15. 1133+432 at 2.3 GHz, the restoring beam is 7.8×4.8 mas in PA -1.3° , the rms noise on the image is 1.7 mJy/beam, the lowest contour is 2.4σ , the peak flux density is 560 mJy/beam.

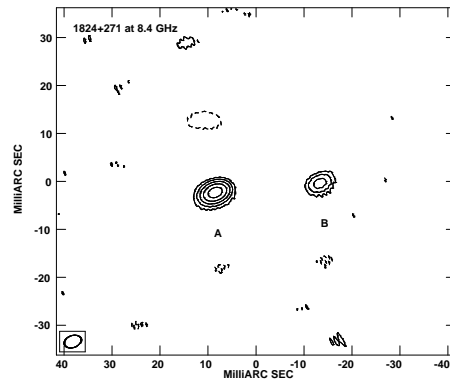


Fig. 18. 1824+271 at 8.4 GHz, the restoring beam is 2.7×1.9 mas in PA -70° , the rms noise on the image is 0.4 mJy/beam, the lowest contour is 2.5σ , the peak flux density is 24 mJy/beam.

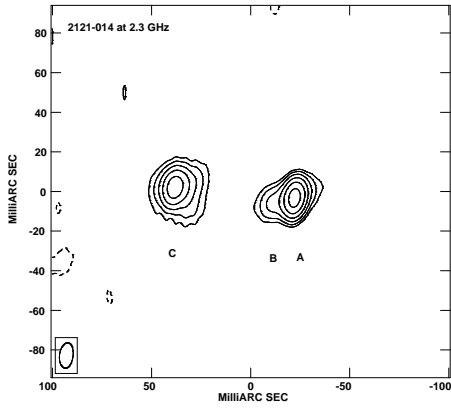


Fig. 19. 2121–014 at 2.3 GHz, the restoring beam is 12.9×6.8 mas in PA -6.8° , the rms noise on the image is 2.3 mJy/beam, the lowest contour is 2.6σ , the peak flux density is 276 mJy/beam.

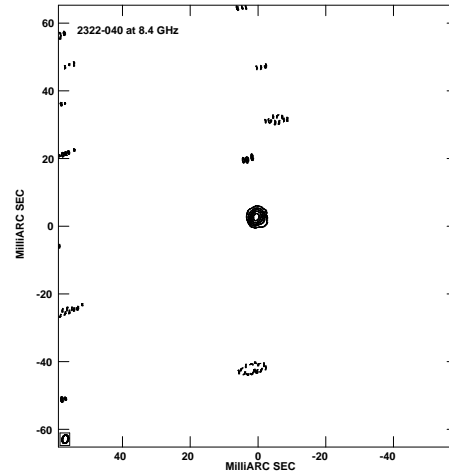


Fig. 22. 2322–040 at 8.4 GHz, the restoring beam is 2.5×1.7 mas in PA -13° , the rms noise on the image is 1.6 mJy/beam, the lowest contour is 1.9σ , the peak flux density is 125 mJy/beam.

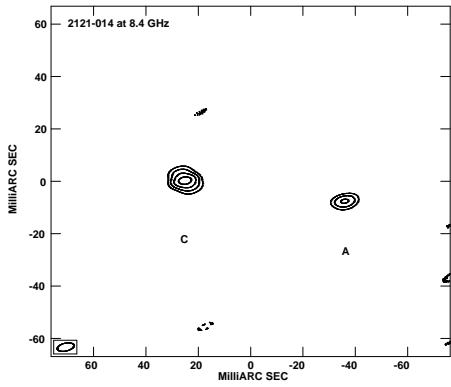


Fig. 20. 2121–014 at 8.4 GHz, the restoring beam is 6.4×3.0 mas in PA -77° , the rms noise on the image is 1.5 mJy/beam, the lowest contour is 4σ , the peak flux density is 70 mJy/beam.

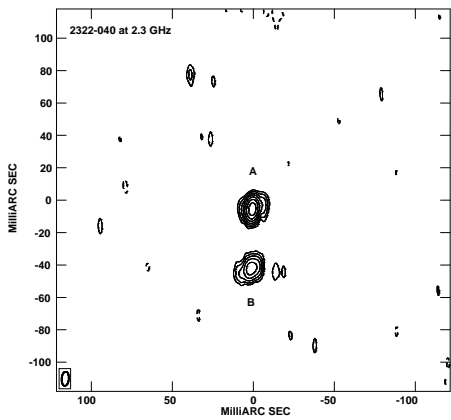


Fig. 21. 2322–040 at 2.3 GHz, the restoring beam is 8.8×4.4 mas in PA -4.5° , the rms noise on the image is 1.6 mJy/beam, the lowest contour is 2.5σ , the peak flux density is 541 mJy/beam.